SCIENTIFIC FLOW-FIELD SIMULATION OF CRUCIFORM MISSILES THROUGH THE THIN-LAYER NAVIER-STOKES EQUATIONS

S. H. Pourtakdoust
Department of Mechanical Engineering
Sharif University of Technology
Tehran-Iran

Abstract The thin-layer Navier-Stokes equations are solved for two complete missile configurations on an IBM 3090-200 vectro-facility supercomputer. The conservation form of the three-dimensional equations, written in generalized coordinates, are finite differenced and solved on a body-fitted curvilinear grid system developed in conjunction with the flowfield solver. The numerical procedure is based on an implicit approximate factorization algorithm employing a multi-grid approach in the simulation of flow about complex finned-missile configurations. The grid program is based on the method of algebraic interpolation and is capable of generating three-dimensional grid systems for missile bodies and finned-missiles having up to eight control surfaces. The multi-grid method improves the CPU time by as much as a factor of 40 over the conventional single-grid method. In addition, using the IBM's vectorizing and optimizing Fortran compiler, speeds up the total execution time (CPU) by more than 90 percent over the same code run on a non-vector architectured machine. The present method is applied to complete missile configurations in supersonic flow at high angles of attack. The predicted aerodynamic coefficients match the available wind-tunnel data with good accuracy. Flow nonlinearities such as shock and separation are detected and verified with the available experimental reports. Body vortex separation and classical patterns of vortical flow are also numerically obtained and examined for vortex interaction effects.

Key Words Flow-Field, Cruciform Missiles, Simulation, Navier-Stokes, Vortex, Aerodynamics, Wind-Tunnel

چکیده معادلات لایه-نازک نویر-استوکز برای دو موشک کامل روی سوپر کامپیوتر IBM مدل ۲۰۰-۳۰۹۰ دارای تسهیلات برداری حل گردیده است. حل این معادلات که در فرم بقاء در مختصات تعمیم یافته مطرح شده اند روی یک شبکه منحنی الخط همگون با هندسه جسم صورت گرفته است. روش محاسباتی براساس یک الگوریتم ضمنی استوار است که از متد تعدد شبکه درحل جریان حول موشک های بالک دار برای تسریع همگرایی استفاده میکند. روش تولید شبکه براساس متد درون یابی جبری میباشد که قادر است برای موشک های صلیبی با دو سری بالک درجلو و عقب به طور اتوماتیک تولید گره محاسباتی نماید. روش تعدد شبکه هزینه زمانی کامپیوتر را تا ۴۰٪ نسبت به روش استوار بریک شبکه تقلیل میدهد. به همین صورت استفاده از تسهیلات برداری و بهینه سازی سیستم سوپر کامپیوتر IBM در قیاس با سیستمهای ساده باعث ۹۰٪ تقلیل درکل زمان اجرا برنامه میگردد. روش فوق درحل جریان مافوق صوت سه بعدی موشکهای بالک دار در زوایای حمله بالا بکار گرفته شده است. ضرائب ائرودینامیکی پیشگویی شده با نتایج تجربی بدست آمده از تونل باد با دقت خوبی قابل مقایسه میباشند. پدیده های غیرخطی جریان نظیر شاک و جدایی توسط این روش بدست آمده که منطبق بر گزارشات تجربی میباشند. پدیده جدایی گردابه های بدنی و طرح های کلاسیک گردابه ها نیز ازاین روش محاسبه ای درمیدان جریان بدست آمده اند که برای بررسی اثرات اندرکنش و تداخل استفاده شده اند.

INTRODUCTION

The demand on missiles for greater maneuverability requires flying through larger angles of attack, thus making modern missiles' aerodynamics highly concerned with nonlinearities. These nonlinearities are in principle associated with compressibility and vortices which form on the missiles' bodies and fins at high angles of attack. One of the important nonlinear phenomenon in missile aerodynamics is vortex interaction involving forebody and fins. The vortices from the forebody, canard surfaces and aft-body could significantly influence the tail fins, thus affecting the missile longitudinal as well as lateral-directional characteristics. With various combinations of

roll angles, angles of attack and control deflections, the vortex flow at the tail location can become very complex showing highly nonlinear characteristics.

Prediction techniques for these complex nonlinear phenomena in existence today fall into two categories. One is to employ potential flow solutions and vortex modeling [1], and the other is the numerical solution of fluid dynamics equations. In this study, the second approach will be used. Most of the numerical aerodynamic simulations for complete missile configurations have been based on Euler solutions [2-5]. One expected problem with the Euler method is the prediction of boundary-layer separation and vortex separation on a smooth-surfaced body where separation locations are unkonwn a priori and cannot be predicted by an inviscid method. On the other hand, Navier-Stokes methods are inherently capable of modeling all physical flow mechanisms, including flow separation. For example, Marconi and Wilson [6] applied a thin-layer Navier-Stokes method to the calculation of leeside flowfield of a cone at an angle of attack and showed good agreement with experimental data. Navier-Stokes solutions for an elliptic-body missile at high angles of attack have also been obtained by Newsome and Adams [7]. The computed pressure distributions agreed well with data. Deese, Agarwal and Gielda [8] presented results from a parabolized Navier-Stokes code and a Reynolds-averaged Navier-Stokes code which agreed well with experimental pressure distributions and total forces and moments. However, these calculations have not specifically addressed the phenomenon of vortex interaction. In addition, Navier-Stokes calculations are very CPU intensive and any practical method to reduce the CPU time would be useful.

In this study, solutions of the thin-layer Navier-Stokes (TLNS) equations are obtained for two realistic missile configurations in supersonic flow at high angles of attack. To increase the solution convergence, a multi-grid strategy is applied in the surface-normal direction allowing the numerical solution to start with a coarse grid system and advance toward the steady-state solution with larger time steps. This would capture the far-field solutions, and as the iterative process continues with finer grid sequences, an overall converged solution to the entire flowfield is obtained. In addition, by taking advantage of the IBM's 3090 vectorizing and optimizing Fortran compiler, substantial reduction in the CPU time (more than 90 percent) is achieved with minimal effort in vectorizing portions of the code.

THEORETICAL DEVELOPMENT

The solver code used in this investigation is developed as an extension of Pulliam [9] for the simulation of complete finned-missile configuration. To allow prediction of missiles' aerodynamics the code is provided with a three-dimensional grid-generator code capable of handling up to an eight-surface missile. To improve the solution convergence a multi-grid approach is followed with one degree of freedom in the direction normal to the missile surface. Aside from prediction of nonlinearities associated with missiles' aerodynamics at high angles of attack, missile designers also often interested in missiles' aerodynamic loadings. Therefore, the code is finally supplemented with a 3-D numerical integration scheme which performs the pertinent loading computations in the physical domain.

Governing Equations

The thin-layer Navier-Stokes equations are written in generalized coordinates [9]:

$$\frac{\partial Q}{\partial \tau}+\frac{\partial E}{\partial \xi}+\frac{\partial F}{\partial \eta}+\frac{\partial G}{\partial \zeta}=Re^{-1}\left[\frac{\partial S}{\partial \zeta}\right] \qquad (1)$$

Where:

$$Q=J^{-1}\begin{bmatrix}\rho\\ \rho u\\ \rho v\\ \rho w\\ e\end{bmatrix} \qquad E=J^{-1}\begin{bmatrix}\rho U\\ \rho uU+\xi_x P\\ \rho vU+\xi_y P\\ \rho wU+\xi_z P\\ U(e+P)-\xi_t P\end{bmatrix}$$

1(a)

$$F=J^{-1}\begin{bmatrix}\rho V\\ \rho uV+\eta_x P\\ \rho vV+\eta_y P\\ \rho wV+\eta_z P\\ V(e+P)-\eta_t P\end{bmatrix} \qquad G=J^{-1}\begin{bmatrix}\rho W\\ \rho uW+\zeta_x P\\ \rho vW+\zeta_y P\\ \rho wW+\zeta_z P\\ W(e+P)-\zeta_t P\end{bmatrix}$$

$$S = J^{-1}\begin{bmatrix} 0 \\ \mu m_1 u_\zeta + (\mu/3) m_2 \zeta_x \\ \mu m_1 v_\zeta + (\mu/3) m_2 \zeta_y \\ \mu m_1 w\zeta + (\mu/3) m_2 \zeta_z \\ \mu m_1 m_3 + (\mu/3) m_2 (\zeta_x u + \zeta_y v + \zeta_z w) \end{bmatrix} \qquad 1(b)$$

with

$$m_1 = (\zeta_x)^2 + (\zeta_y)^2 + (\zeta_z)^2$$

$$m_2 = \zeta_x u_\zeta + \zeta_y v_\zeta + \zeta_z w_\zeta \qquad 1(c)$$

$$m_3 = 0.5\left[\frac{\partial}{\partial \zeta}(u^2 + v^2 + w^2)\right] + Pr^{-1}(\gamma - 1)^{-1}\frac{\partial a^2}{\partial \zeta}$$

Note that in Equation (1) Q is the solution vector, E,F and G are the inviscid flux vectors, S is the viscous flux vector and Re is the Reynolds number. The coordinates (x,y,z) define the physical domain while (ξ, η, ζ) are the corresponding coordinates in the computational domain. The contravariant velocity components (U, V, W) in Equations 1(a) are defined as follows:

$$\begin{aligned} U &= \xi_t + \xi_x u + \xi_y v + \xi_z w \\ V &= \eta_t + \eta_x u + \eta_y v + \eta_z w \qquad (2) \\ W &= \zeta_t + \zeta_x u + \zeta_y v + \zeta_z w \end{aligned}$$

Equation (1) is solved through finite difference approximation using the Beam-Warming implicit approximate factorization algorithm [10], where all spatial derivatives are central differenced and the time integration can be either first or second order accurate. The resulting factored Equation (3) produces three one-dimensional operators which are solved one direction at a time. This procedure generates block tri-diagonal matrix systems (easier to solve) for each space variable which are solved using the method of block lower-upper decomposition (LUD).

$$(I + h\delta_\xi A^n + D_\xi^{(2)})(I + h\delta_\eta B^n + D_\eta^{(2)})(I + h\delta_\zeta C^n - h\,Re^{-1}\delta_\zeta M^n + D_\xi^{(2)})\,\Delta Q^n = -h(\delta_\xi E^n + \delta_\eta F^n + \delta_\zeta G^n - Re^{-1}\delta_\zeta S^n + D^{(4)}) \qquad (3)$$

where A,B,C,D are flux jacobian matrices $\partial E/\partial Q$, $\partial F/\partial Q$, $\partial S\partial Q$ respectively and are obtained by differentiating the flux vectors with respect to the vector of flow variables Q. To maintain numerical stability, artificial dissipation terms must be added, since a central differencing scheme is being used [11]. Consequently, an explicit fourth-order dissipation term is added to the flux calculations and an implicit second order dissipation term is added to each block tri-diagonals of Equation (3) to damp out high-frequency growth and control nonlinear instability.

Boundary Conditions

Specification of the flow variables on the rigid body surface (inner boundary) and on the outer boundary points constitutes the required boundary conditions. For viscous flow, the no-slip conditions, U = V = W = 0 are enforced on missile surface $\zeta(x,y,z,t) = 0$. The flow tangency condition, W = 0, is utilized on the missile surface in inviscid flow. The body surface-pressure is obtained from a relation derived from the normal momentum Equation (12) which results in computed pressure normal to the body surface. The density and total energy values are obtained using constant free-stream stagnation enthalpy H_0 condition along the body in inviscid flow and adiabatic wall condition in viscous flow. In supersonic flow, the outer-bondary flow variables are set to their free-stream values and are kept constant at all time levels until steady-state solution or convergence to desired accuracy is achieved.

Numerical Grid Generation

Generation of a single grid system for a realistic configuration is a major problem in CFD (Computational Fluid Dynamics) calculations. Although several codes are available for application, such as Thompson's "EAGLE" code [13], they are not automated enough for missile work and have extensive input requirements. Therefore, a numerical grid generator code suitable for missile applications is developed. Additional desired features of this code are user friendliness and simplicity of data structure. The code is based on the method of algebraic interpolation and is capable of generating a single-block three-dimensional grid system for missile configurations with up to eight control surfaces (Figure 1). In general, the following principles are upheld in generation

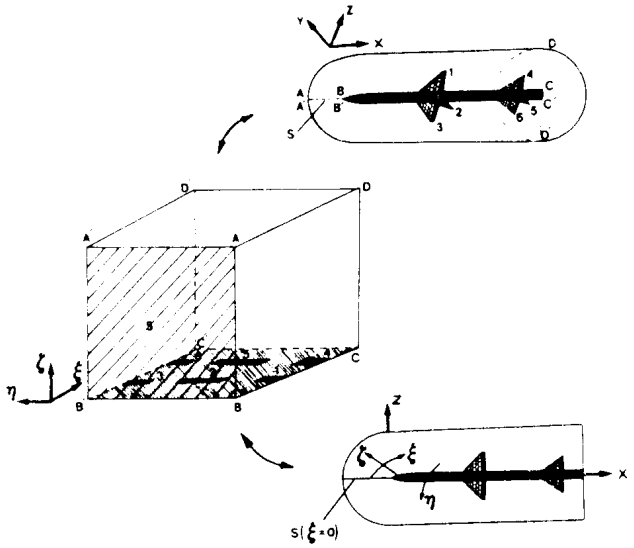

Figure 1. Physical and computational domains

of the grid systems:

1. The generated grids conform to the boundaries of the region of interest;

2. The grids are concentrated in the regions where high gradients in the solutions are expected;

3. The generated grids provide orthogonality or near-orthogonality of the surface coordinates at the mesh points.

For any missile-type body consisting of a forebody portion followed usually by a long cylindrical afterbody, variable grid concentrations in axial (streamwise) direction are produced to furnish more grids in the forebody portion. The body cross-section could be either circular or elliptical. The missile sideline contour (top view) is the only required input to the program which could be supplied via either equations or a collection of coordinates. The grids are computed upon specification of the required grid size in the axial (streamwise), circumferential (around the body) and normal directions. The grid spacing in normal directions is exponentially varied to allow grid concentration close to body surface.

On portions of the missile where the control surfaces are located, the grids are computed for a series of cross-sectional geometries. These cross-sectional grids will eventually be aligned along a single axis to produce a unified mesh for the entire missile. The missile wings (fins) could be either of slab type or of elliptic cross-section where the number of axail cross-sections along a set of control surfaces is arbitrary and usually configuration dependent. To provide near orthogonality of the surface coordinates at the mesh points, fin grid points depart from the surface parabolically toward the outer boundary. These parabolic curves are parameterized with respect to arc length to allow exponential spacing. Figure 2 shows typical examples of computational grids for a cruciform missile.

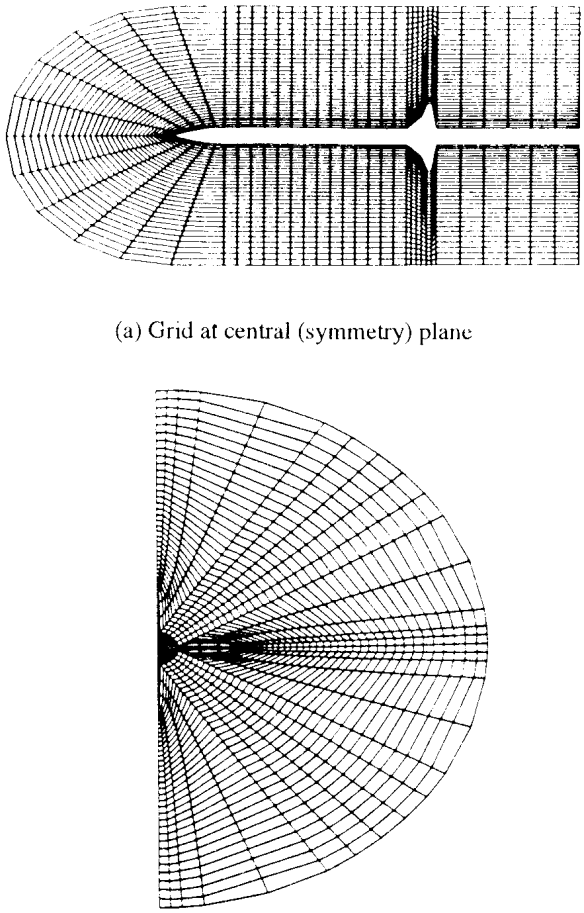

(a) Grid at central (symmetry) plane

(b) Cross-sectional grid

Figure 2. Computational grid for a cruciform missile

Computational Time Survey

Table 1 shows a survey of the CPU times corresponding to various cases that have been studied. As noticed, the key factors in the reduction of the CPU time are the computational power of the computer (about 130 MFLOPS for IBM-3090 [14]) and the accelerated convergence rate of the multi-grid approach. The combination of computer power and the multi-grid approach produced more than 90 percent reduction in the CPU time as the IBM results are

TABLE 1		Computer Time Survey		
Configuration	**No. of Grids**	**Approach**	**Computer**	**CPU (HR)***
Missile Body	17,100	Single-Grid	Harris-1200	16.00
Missile Body	17,100	Multi-Grid	Harris-1200	10.00
Missile Body	17,100	Single-Grid	IBM-3090	1.60
Missile Body	17,100	Multi-Grid	IBM-3090	0.96
Complete Missile (4-Surface)	43,296	Multi-Grid	IBM-3090	2.64
Complete Missile (8-Surface)	50,688	Multi-Grid	IBM-3090	3.10

*Based on same level of convergence

compared with those of Harris-1200, a relatively low performance computer, even though minimal effort was spent vectorizing portions of the code.

DISCUSSION OF RESULTS

In this paper the results of the numerical simulations of two complete missile configurations will be presented. The maximum number of grids considered was 50,688 consisting of 48 axial points, 33 circumferential points and 32 points in radial (normal) direction with bilateral symmetry imposed. The following sections present detailed results.

A Four-Surface Cruciform Missile {MISSILE(1)}

This configuration matches that of Reference 15 for which some experimental loading results are available. Figure 3 shows the geometry of this missile with the surface grids. For ease of reference, this configuration will be called MISSILE(1) from here on. MISSILE(1) was tested at three Mach numbers of 2.36, 1.60 and 1.20. Computations were done for a range of angles of attack at M= 2.36 for loading comparisons. MISSILE(1) was also analyzed at a roll angle of 45° at a free-stream Mach number of 1.6. The laminar viscous-flow Reynolds number used for all runs was 502, 920 (6.6×10^6/m) based on the body diameter of 0.25 feet (7.62 cm) in accordance with the available experimental test conditions [15].

The first run was made at M= 2.36 and 20.82° of angle of attack. At this combination of Mach number and Reynolds

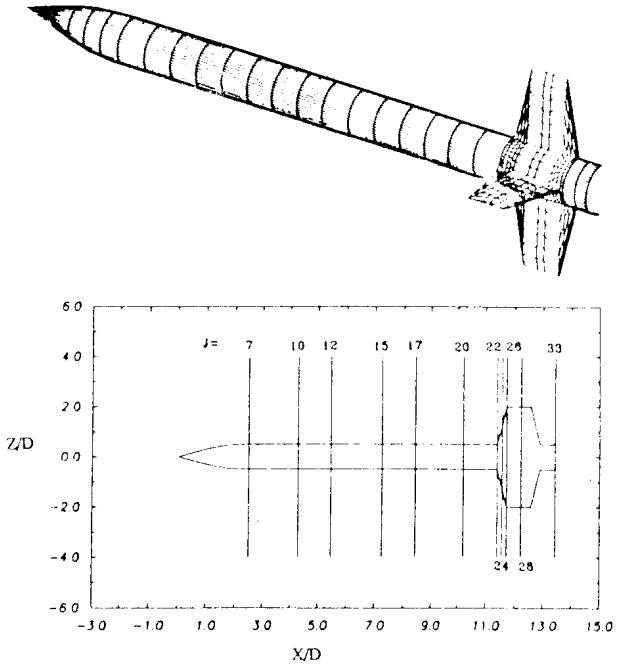

Figure 3. Geometry of MISSILE(1) with surface grids and locations of streamwise stations.

number, the flow is shock dominated and the boundary layer is thin and difficult to resolve. Furthermore, the complex missile geometry with fins (low-sweep) perceived as sharp discontinuities in the flow field, made convergence with a single-grid system almost impossible. Consequently, a multi-grid approach is followed where three grid sequences are used until convergence to the second order of residuals is achieved. Figure 4 shows that the multi-grid method reduces the residuals by a factor of 10^{-3} smaller than that

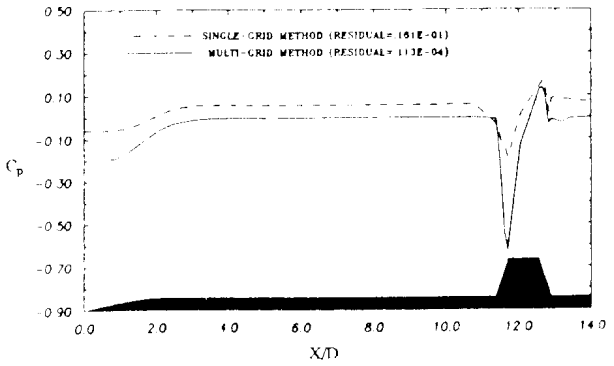

Figure 4. Effect of multi-grid approach on the computed pressure distribution of MISSILE(1) on the plane of symmetry at M= 2.36, α= 20.82 deg. and Re= 502, 920 for zero roll angle.

10^{-3} smaller than that given by a single-grid method at the same number of iterations (3700). The sequential grid system maintains the same number of grid points in the axial (41) and circumferential (33) directions and allows for a varying number of grid points in the normal (radial) direction. In this case, the number of grid points in the normal direction varied from 10 (coarse) to 21 (finer) and finally to 32. Using the multi-grid method, the areodynamic loading coefficients are calculated as functions of angle of attack and compared with data in Figure 5. The results are in good agreement with the experimental data [15] with 90 percent accuracy in the lift and drag coefficients at high angles of attack. The pitching-moment coefficient is within 85 percent of its experimental value. Figure 6 indicates the occurrence of a bow shock close to the body nose. As mentioned earlier, at this Mach number (2.36) the flow is mostly shock dominated, and no vortex flow is detected. The shock locations and the relatively thin boundary layer are noticeable in the flowfield plots of Mach number and pressure shown in Figure 7. At a lower free-stream Mach number of 1.6, still no strong vortex flow is detected. This could be attributed to the high flow Reynolds (6.6×10^6/m) used in this simulation. At this Mach number (1.6), the flow is characterized by a bow shock structure starting close to the body nose (Figure 8) and continuing downstream toward the aft control surfaces. To see the roll effect on the flowfield, two cross-flow fringe plots of Mach number and pressure at an axial location X/D= 11.73 (J= 26) are shown in Figures 9 and 10. Higher pick pressures are computed for the case of 45° roll. Figure 11 shows the surface pressure distribution at zero roll, indicating low pressure regions prevailing on the missile upper surface.

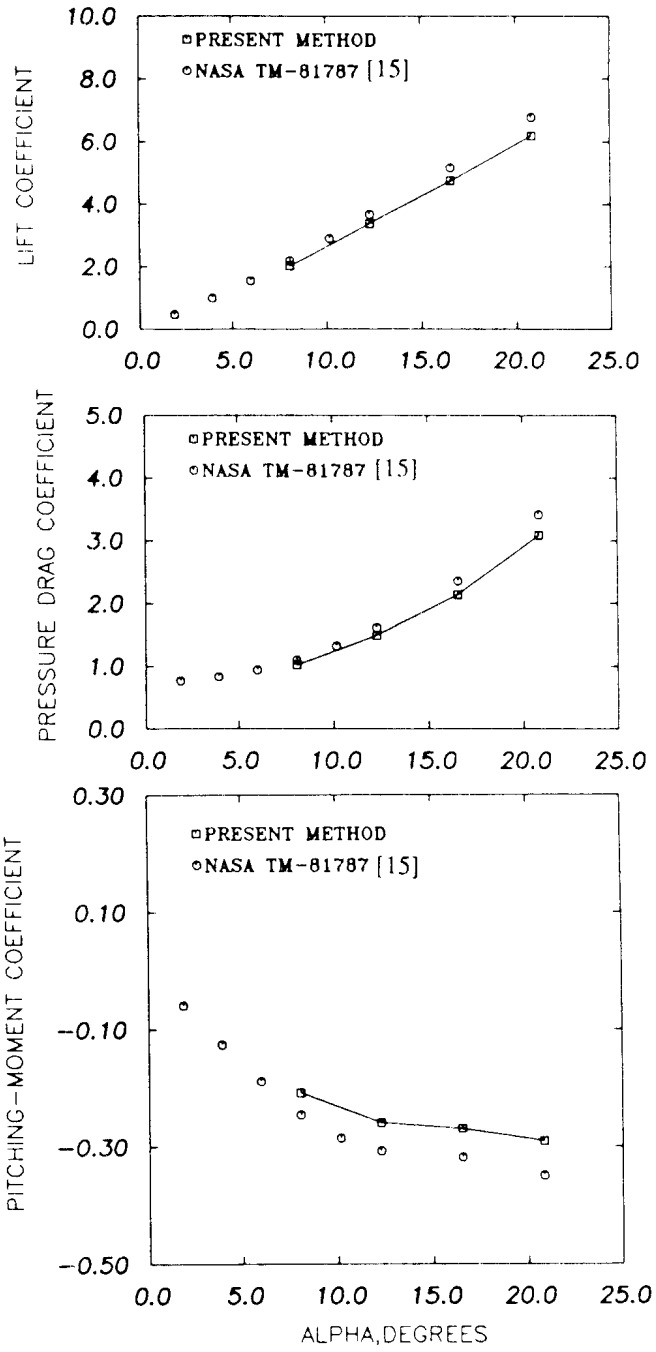

Figure 5. Aerodynamic characteristics of MISSILE(1) at M= 2.36 and zero roll, Re= 502, 920. Moment center at 62. 15% of body length from nose.

The high-pressure areas are concentrated at the missile nose (lower-surface) and the leading-edges of the control surfaces.

To demonstrate vortex interaction, a lower supersonic Mach number is needed. For this purpose, a condition with M= 1.2 and α= 20.24° is considerd with zero roll and 45°

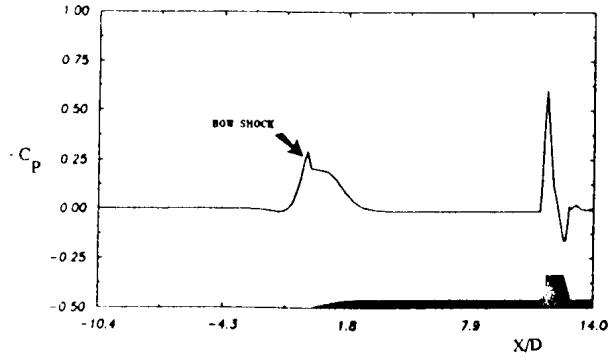

(a) Leeward side

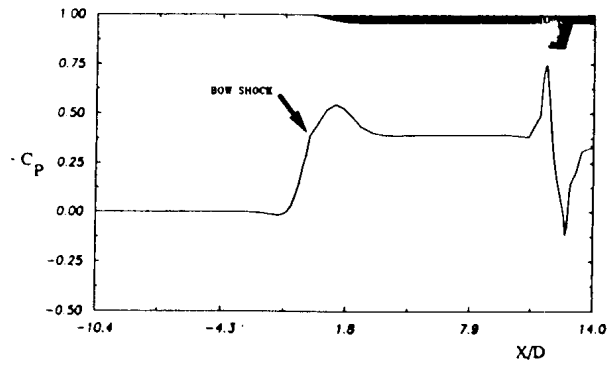

(b) Windward side

Figure 6. Computed pressure distribution in the plane of symmetry for MISSILE(1) at M= 2.36, α= 20.82 deg. and zero roll.

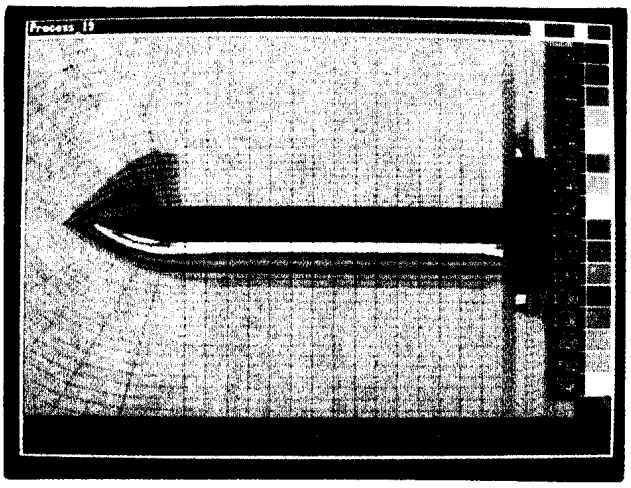

(a) Pressure distribution

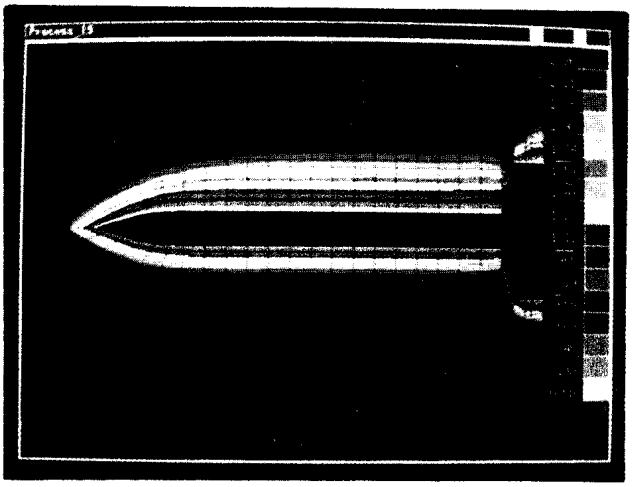

(b) Mach number distribution

Figure 7. Mach number and pressure distributions in the plane of symmetry of MISSILE(1) at M= 2.36, α= 20.82 deg. and zero roll.

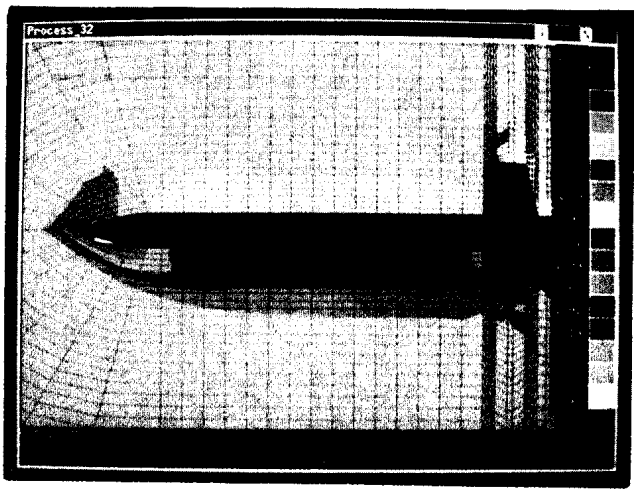

(a) Pressure distribution

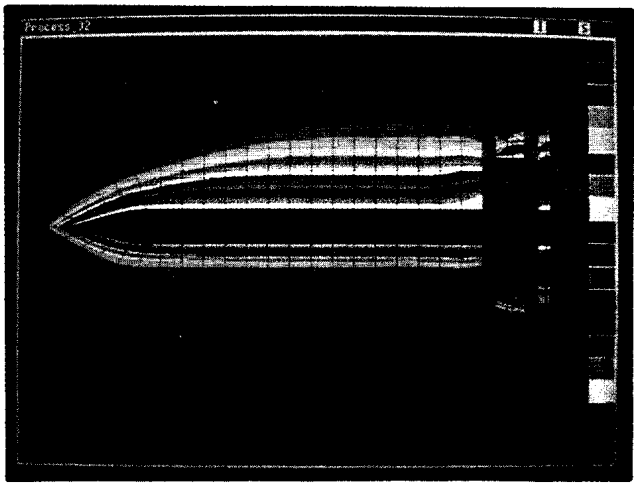

(b) Mach number distribution

Figure 8. Mach number and pressure distributions in the plane of symmetry of MISSILE(1) at M= 1.6, α= 20.24 deg. and zero roll

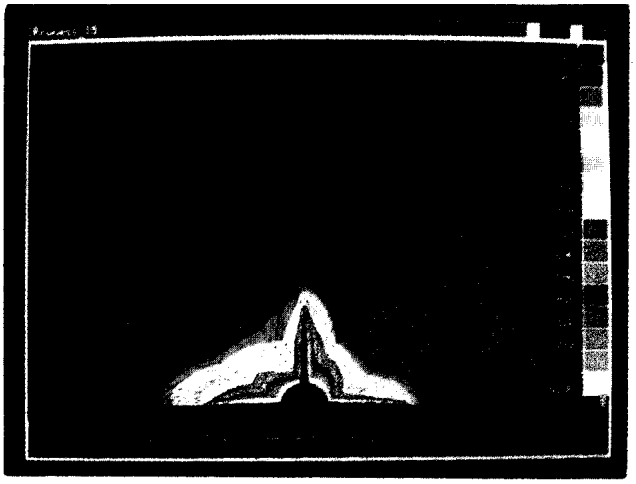

(a) Mach number distribution

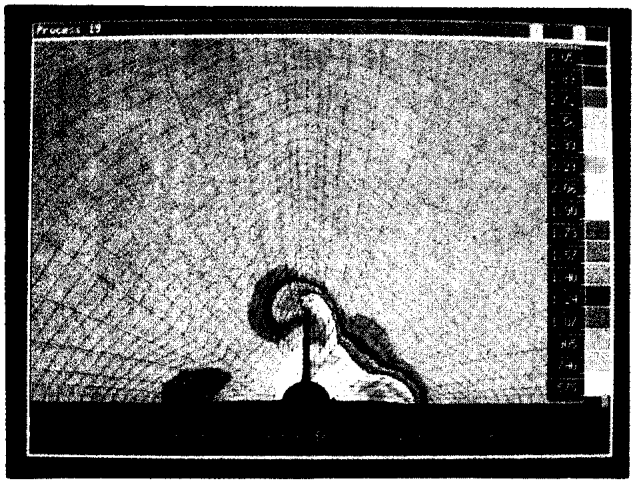

(b) Pressure distribution

Figure 9. Mach number and pressure distributions in the cross-flow plane for MISSILE (1) at M= 1.6, α= 20.24 deg. and zero roll. X/D= 11.73 (J= 26)

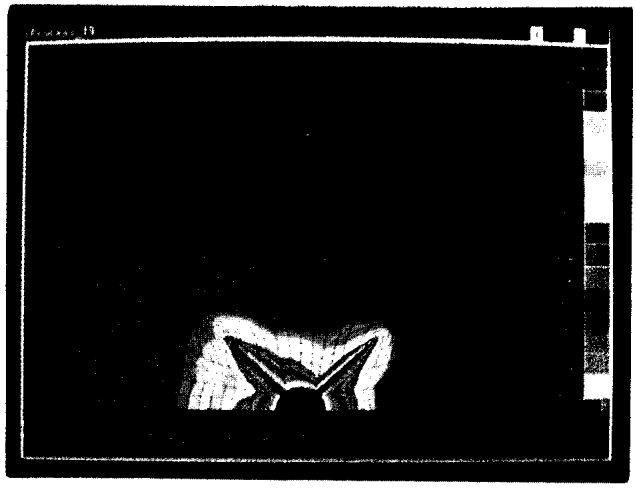

(a) Mach number distribution

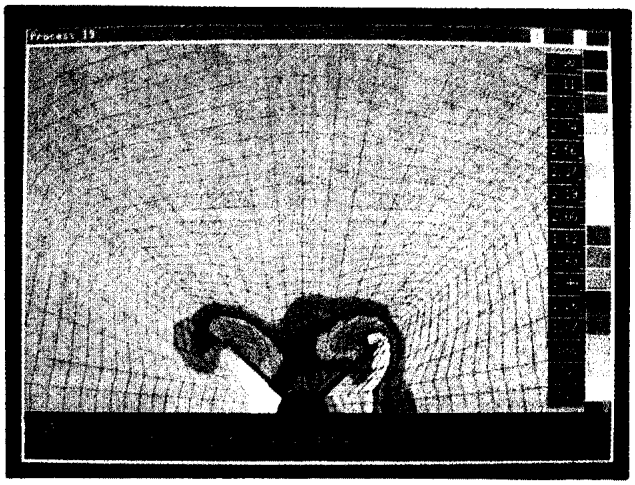

(b) Pressure distribution

Figure 10. Mach number and pressure distributions in the cross-flow plane for MISSILE (1) at M= 1.6, α= 20.24 deg. and 45° roll. X/D= 11.73 (J= 26).

roll angles. The results in the form of velocity vector plots in the cross-flow planes show vortex formation on the leeward side of the body surface which starts at a downstream location of X/D= 7.25 and continues downstream throughout the entire missile length. Note that no experimental flowfield data are available for comparison. Comparing the velocity plots at stations before and over the fins at zero roll angle (Figures 12(a) and 12(b)), interaction of forebody vortices with the fins is noticeable. It is seen that the fins have an adverse effect on the forebody vortices, causing rapid diffusion. This is further verified by a smoother and nearly constant pressure-distribution on the upper surface at X/D= 11.73 (Figure 13). Behind the fins, the forebody vortex tends to regroup (Figure 14). Results at a roll angle of 45° are presented in Figure 15. Because of the shock effect, the vortex flow at a station slightly ahead of the fin-leading edge is considerably weaker and totally diffused over the fins. Again, the vortex flow reappears behind the fins (Figure 15(c)).

An Eight-Surface Sparrow Missile {MISSILE(2)}

This configuration is illustrated in Figure 16 along with the

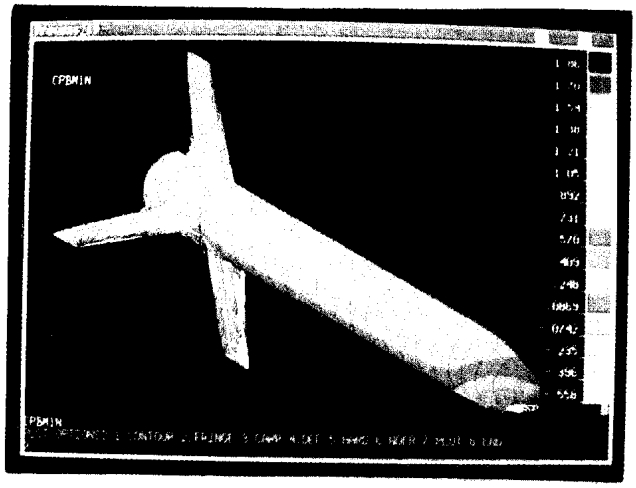

(a) Leeward side

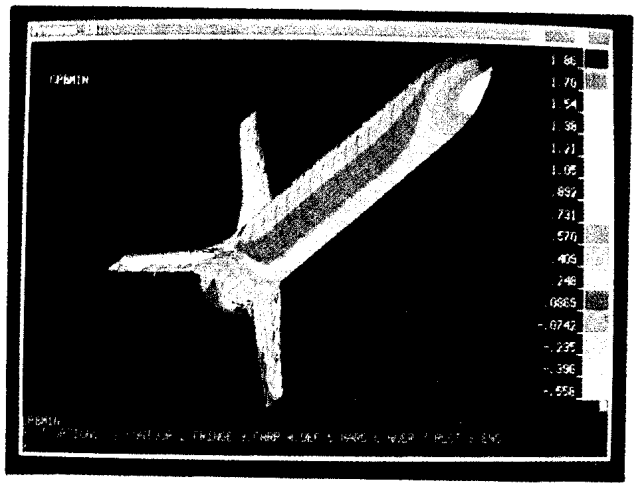

(b) Windward side

Figure 11. Distribution of surface pressure coefficients for MISSILE (1) at M= 1.6, α= 20.24 deg. and zero roll.

surface grids. The configuration (referred to as MISSILE(2)) consists of an ogive-cylinder body with cruciform wings and in-line tails. The wings (front fins) have trapezoidal planform with a leading-edge sweep of 45° [16]. The tails (aft fins) have delta-shaped planforms with a leading-edge sweep of 57°. To be compatible with the experimental test conditions at high angles of attack [16], a laminar viscous-flow Reynolds number of 149,961 (4.92×10^6) has been used based on the missile body diameter of 0.1 feet (3.048 cm). The sequential grid system used for MISSILE (2) consists of a ($48 \times 33 \times 21$) mesh structure followed by a ($48 \times 33 \times 32$) grid system, where 48 is the number of axial grid points, 33 is the number of

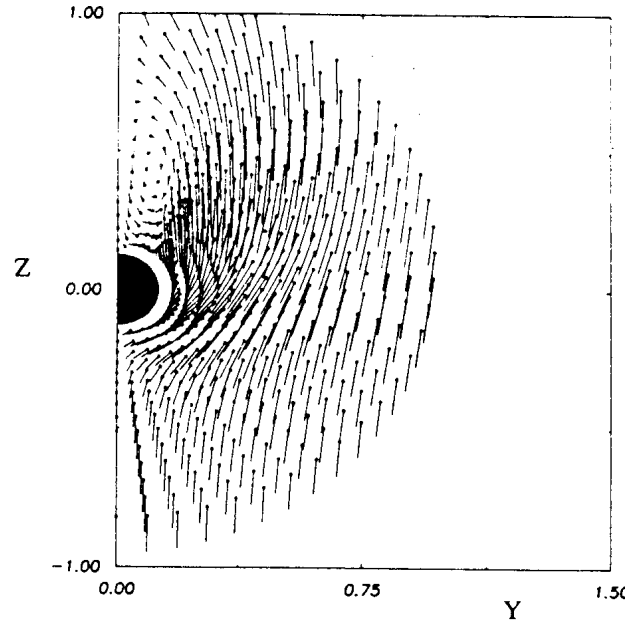

(a) X/D = 11.40 (J=22)

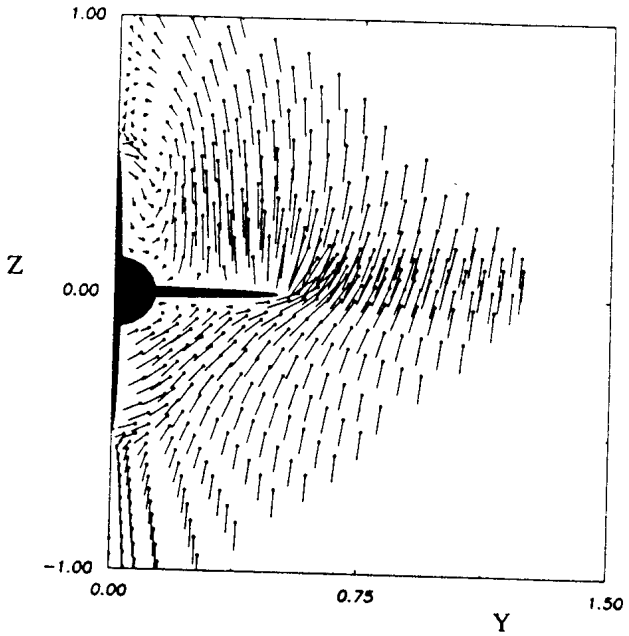

(b) X/D = 11.73 (J=26)

Figure 12. Velocity vector plots in the cross-flow plane fo MISSILE (1) at M= 1.2, α= 20.24 deg. and zero roll angle.

circumferential grid points and 32 represents the number of grids in the normal (radial) direction.

MISSILE(2) is numerically tested at a free-stream Mach number of 1.5 with zero and 45° angles of roll, where computations for both cases are done at a few angles of attack. The loading results for both cases are presented in Figures 17 and 18. Comparisons with experimental data

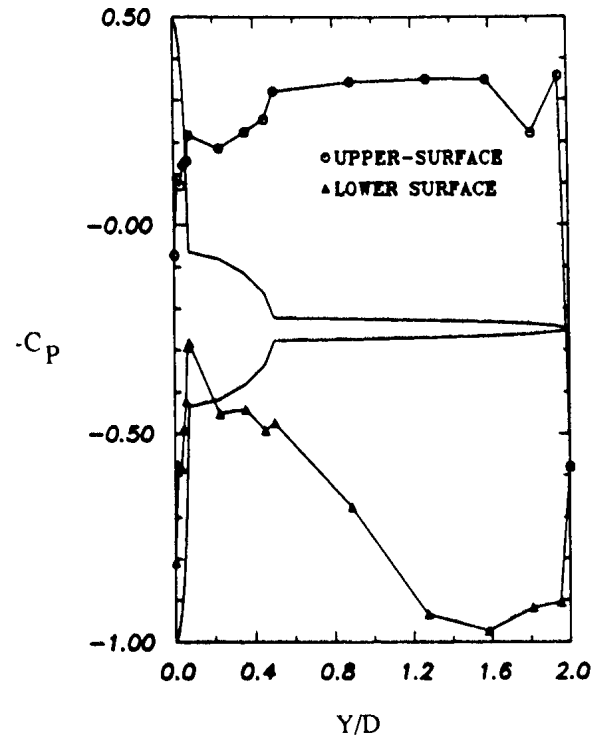

Figure 13. Calculated pressure coefficient for MISSILE(1) at M= 1.2, α= 20.24 deg. and zero roll angle, X/D = 11.73.

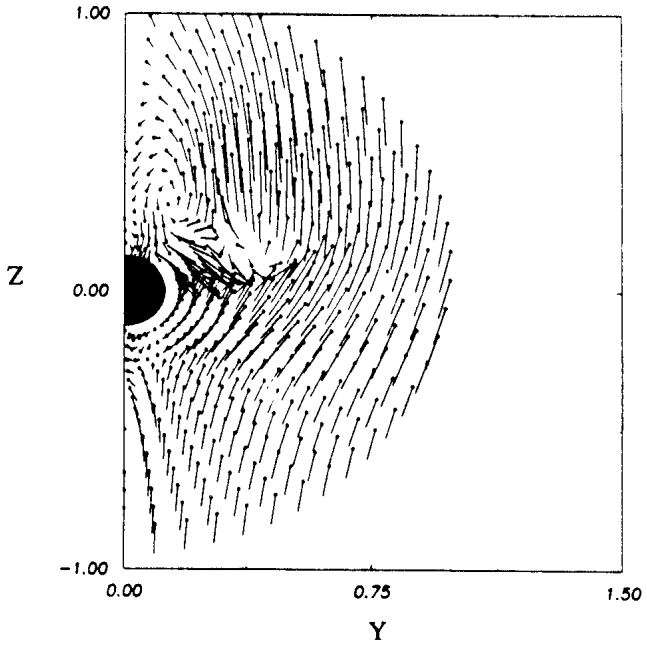

Figure 14. Velocity vector plot in the cross-flow plane for MISSILE(1) behind the aft-fins at M= 1.2, α= 20.24 deg. and zero roll angle, X/D = 12.90 (J= 33).

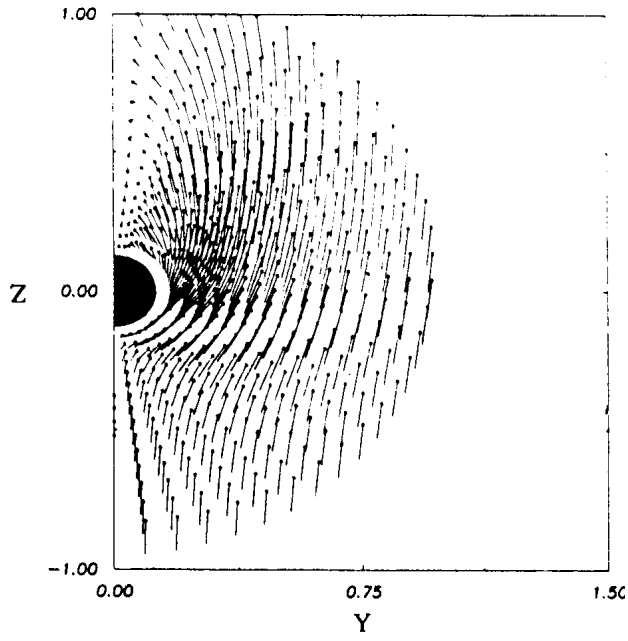

(a) X/D = 11.40 (J=22)

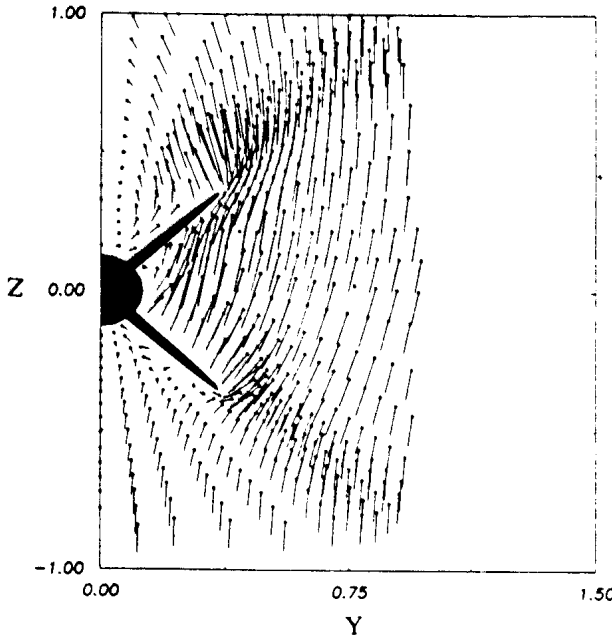

(b) X/D = 11.73 (J=26)

Figure 15. Velocity vector plots in the cross-flow plane for MISSILE(1) at M= 1.2, α= 20.24 deg. and 45 deg. of roll angle

[16] show good accuracy in the prediction of aerodynamic loading coefficients with a 90 percent overall accuracy in the lift and drag coefficients at high angles of attack. The pitching moment coefficient falls between 85 to 90 percent of its experimental value. Even though vortex flow is predicted at these flight conditions, the predicted strength

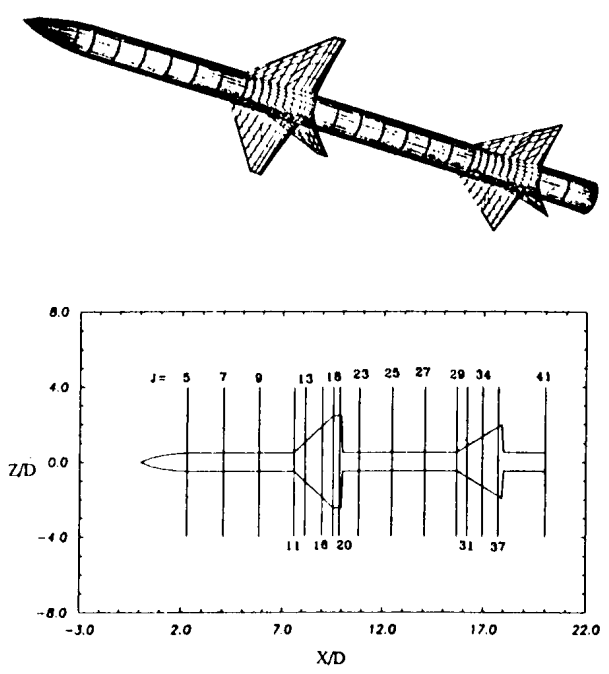

Figure 16. Geometry for MISSILE(2) with surface grids and locations of streamwise stations.

could have affected the uploads on the tail-fin surfaces, causing a discrepancy in the pitching-moment value. Figures 19 and 20 show some cross-flow velocity vector plots for MISSILE(2) at this Mach number (1.5) for both zero and 45° roll angles. Calculations indicate vortex formation on the leeward side starting at X/D= 5.809 (J= 9). At X/D= 8.988 (J= 16) flow separation occurs right at the leading edge of the front control surfaces for both cases. The forebody and wing vortex interaction seem to have a total diffusive effect on the vortices in the flowfield (Figures 19(a)) and 20(a)) which is alleviated downstream of the front surfaces (Figures 19(b) and 20(b)). In the aft-body portion, the vortex interaction has caused a shift of the vortex core further to the right, which is cearly seen at X/D= 14.06 (J= 27) for both cases (Figs. 19(b) and 20(b)). At X/D= 16.97 (J= 34), the body vortex flow and not the leading edge separation dominates the flowfield (Figures 19(c) and 20(c)). Note that for the 45 degree roll angle the vortex becomes vertically elongated (Figure 20(c)) which is also noticeable in the flowfield plots of Figure 21. Downstream of the aft-fins at the missile base (J=41), the vortex core is shifted downwards due to interaction between body and fin vortices (Figures 19(d) and 20(d)). The pressure distribution in the symmetry plane is shown in Figure 22, where the

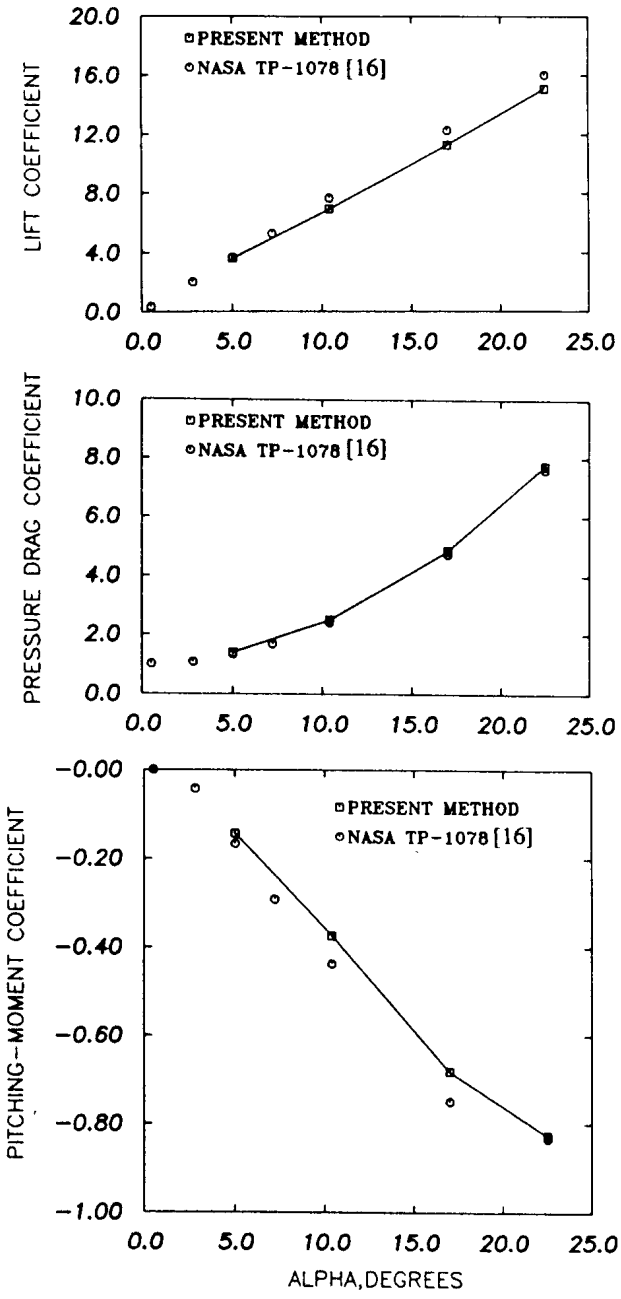

Figure 17. Aerodynamic characteristics for MISSILE(2) AT M= 1.5 and zero roll angle, Re= 149, 961. Moment center at 52. 63% of body length from nose.

rapid increase in the pressure coefficient upstream of the missile body is an indication of a bow shock.

For further qualitative investigation of the interaction phenomenon, MISSILE(2) is also tested at M= 1.2 and 22.5 deg. angle of attack at zero roll angle. At this combination of Mach number and the flow Reynolds number (4.92×10^6

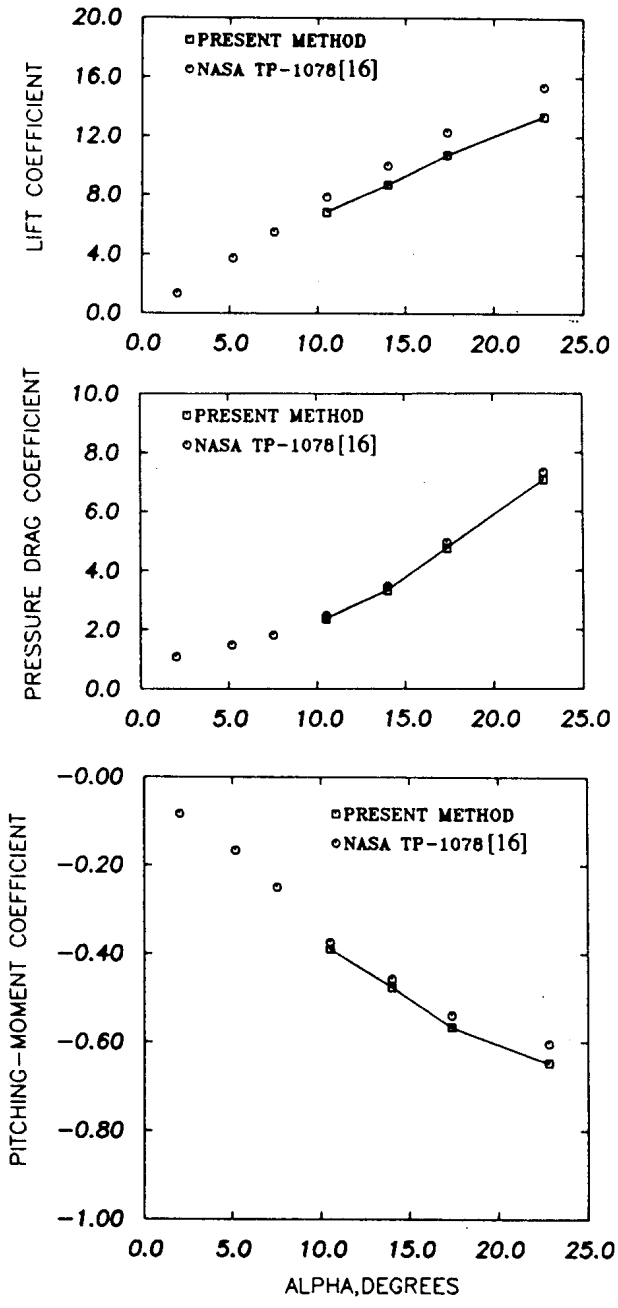

Figure 18. Aerodynamic characteristics for MISSILE(2) AT M= 1.5 and 45 deg. of roll, Re= 149. 961. Moment center at 52. 63% of body length from nose.

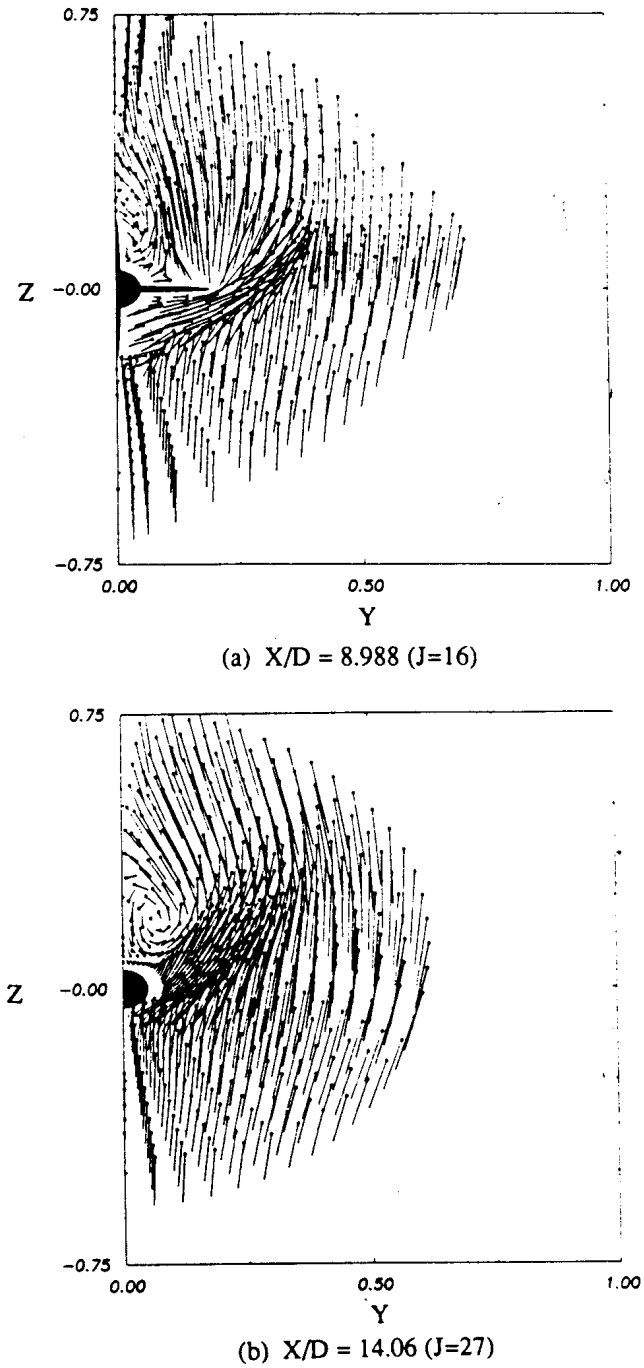

Figure 19. Velocity vector plots in the cross-flow plane for MISSILE(2) at M= 1.5, α= 22.5 deg. and zero roll angle.

m), the flow is vortex-dominated and the viscous layer is relatively thick (Figure 23). The flowfield plots of Figure 24 reaffirm the previous results of interaction, that the combined effect of the vortices coming from the missile forebody and front fins on the aft-body vortex flow, seems to be a rounding of the local vortex flow with a shift of its core further to the right. This, of course, could cause severe control problems in an asymmetric flight condition. At the same Mach number (1.2) the distribution of the surface pressure coefficients is presented in Figure 25 showing low pressure regions prevailing on the leeward side of the missile surface.

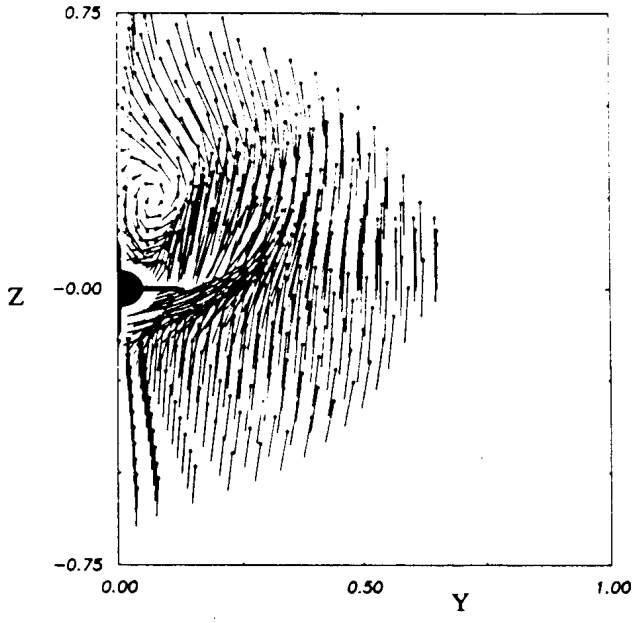

(c) X/D = 16.97 (J=34)

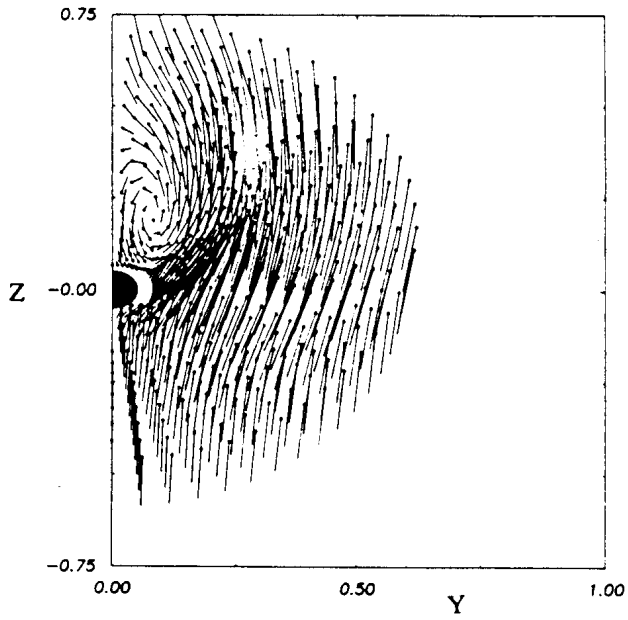

(d) X/D = 20.00 (J=41)

Figure 19. Concluded.

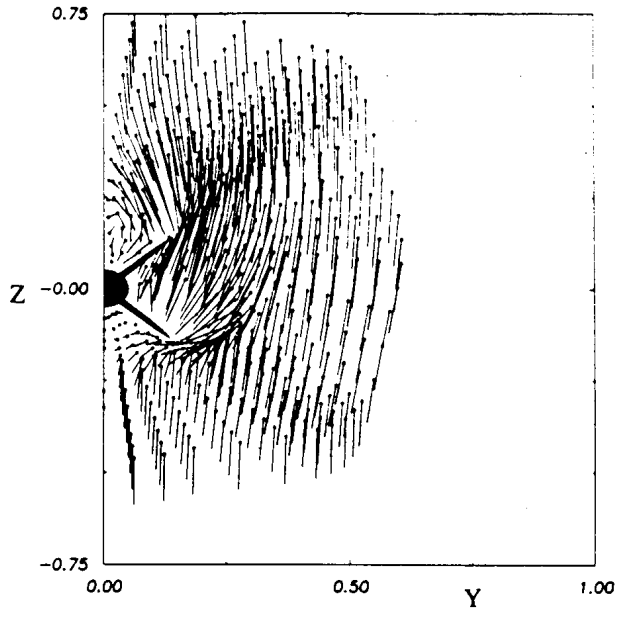

(a) X/D = 8.988 (J=16)

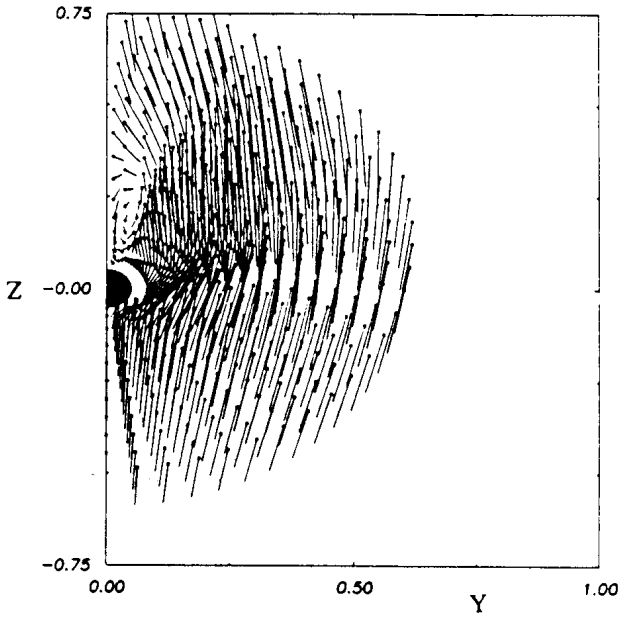

(b) X/D = 14.06 (J=27)

Figure 20. Velocity vector plots in the cross-flow plane for MISSILE(2) at M= 1.5, α= 22.5 deg. and 45 deg. of roll angle.

CONCLUSIONS

The three-dimensional thin-layer Navier-Stokes (TLNS) equations have been solved for two complete missile configurations using the computational power of an IBM 3090-200. The numerical procedure was based on an implicit approximate factorization algorithm employing a multi-grid approach in the simulation of flow about complex finned-missile configurations. Using the IBM's vectorizing and optimizing Fortran compiler with the multi-grid method

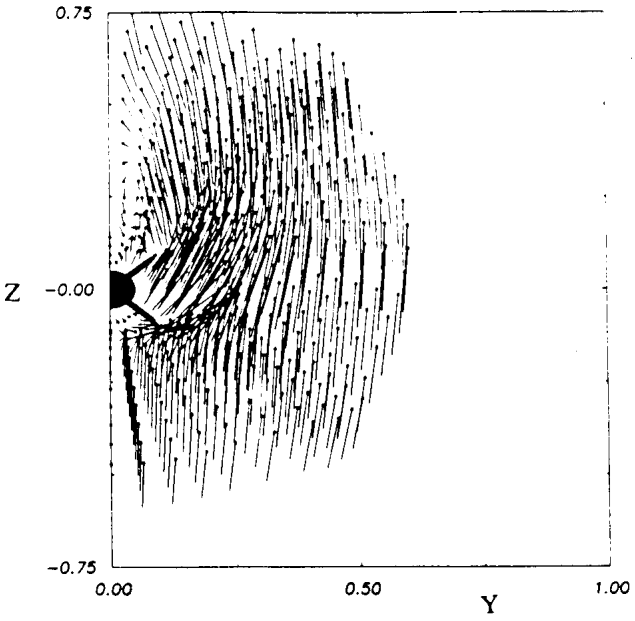

(c) X/D = 16.97 (J=34)

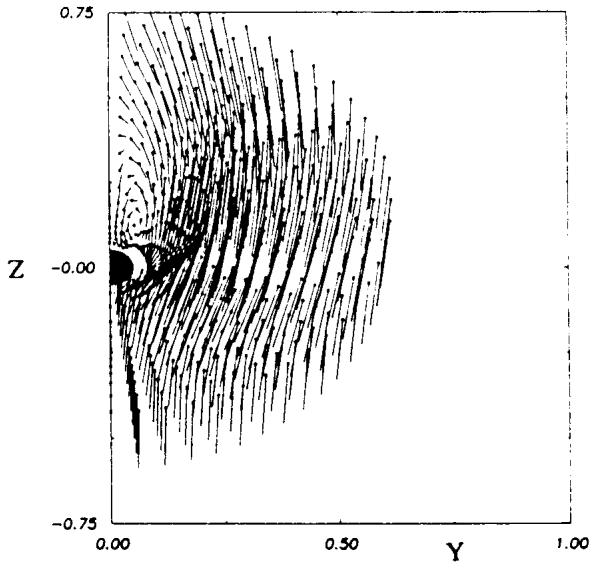

(d) X/D = 20.00 (J=41)

Figure 20. Concluded.

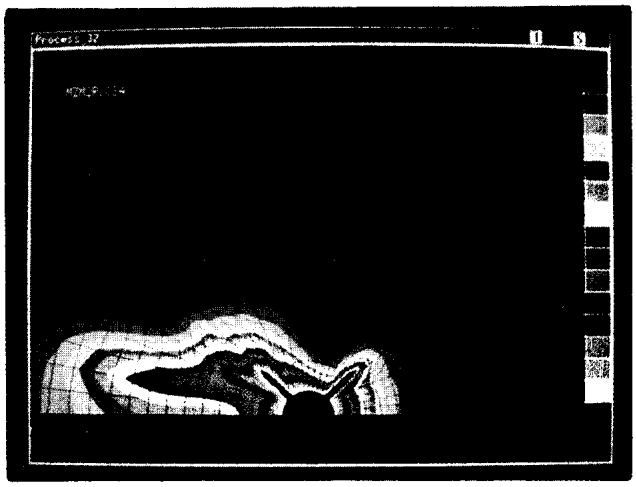

(a) Mach number distribution

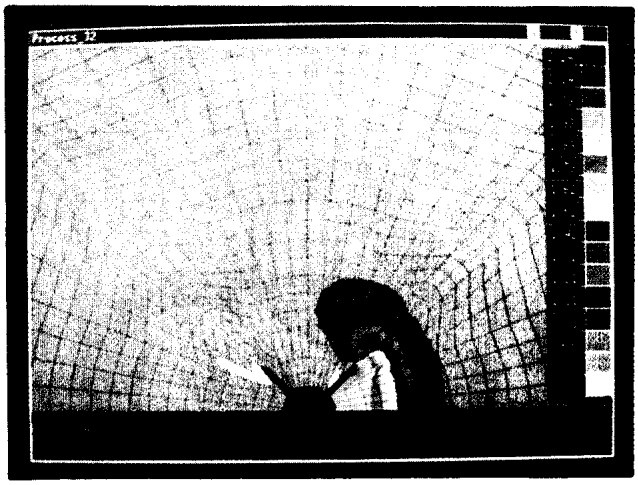

(b) Pressure distribution

Figure 21. Mach number and pressure distributions in the cross-flow plane for MISSILE(2) at M= 1.5, α= 22.5 deg. and 45° roll angle. X/D= 16.97 (J= 34).

sped up the computational time by more than 90 percent over the original code run on Harris-1200 computer.

The numerical results indicate the ability of the TLNS equations to predict complex flowfields about missiles at high angles of attack and roll. In the numerical simulation of the two finned-missiles, the aerodynamic loading coefficients were compared with the available wind tunnel data showing 90-95 percent level of accuracy in the lift and drag coefficients and 80-85 percent accuracy in the pitching moment coefficient. The forebody and fin vortex interaction effects on the flowfield were also qualitatively investigated through examination of the vortical patterns showing elongation and core dislocation. The forebody vortex was shown to diffuse due to the presence of the aft fins and re-form downstream of the fins.

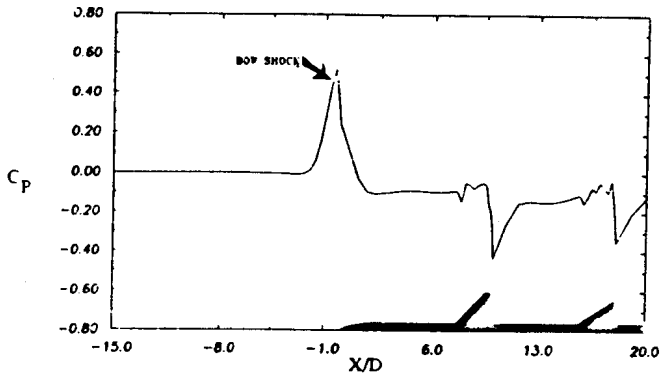

(a) Leeward side

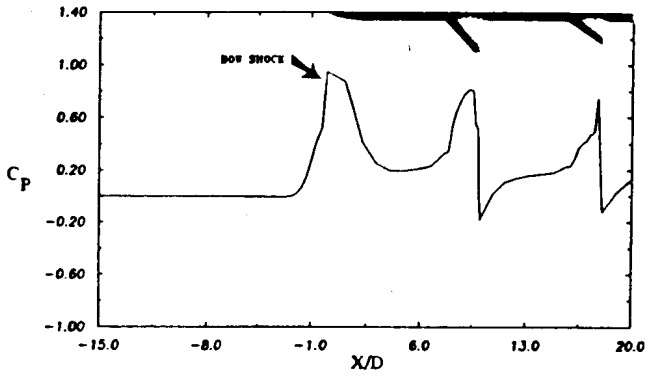

(b) Windward side

Figure 22. Computed pressure distribution in the plane of symmetry for MISSILE(2) at M= 1.5, α= 22.5 deg. and zero roll.

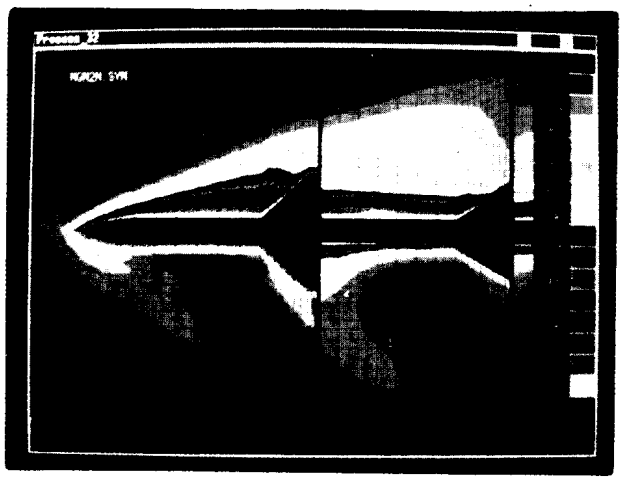

(a) Mach number distribution

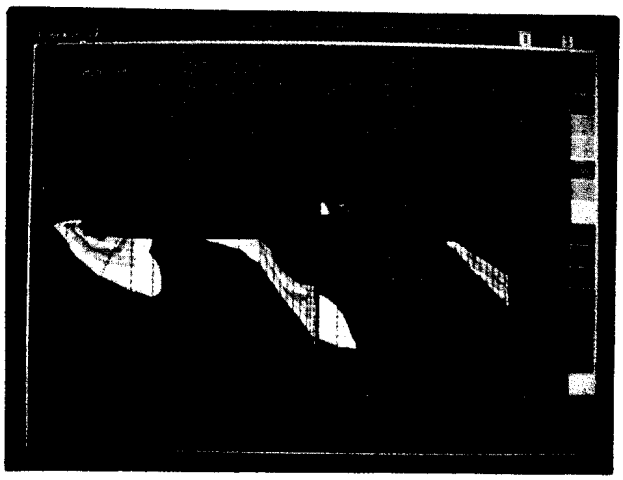

(b) Pressure distribution

Figure 23. Mach number and pressure distributions in the plane of symmetry of MISSILE(2) at M= 1.2,α= 22.5 deg. and zero roll angle.

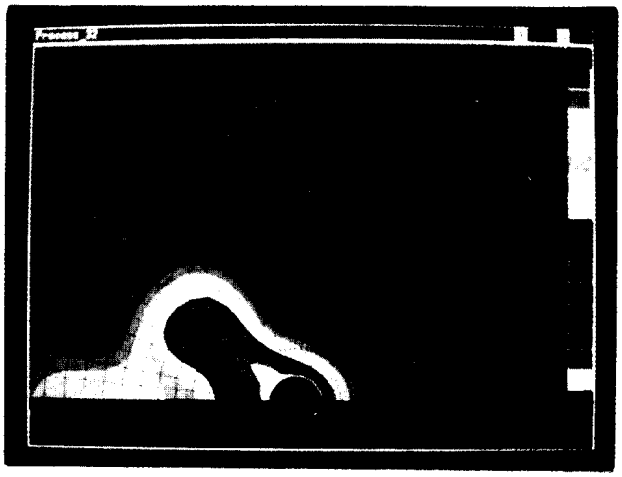

(a) Mach number distribution

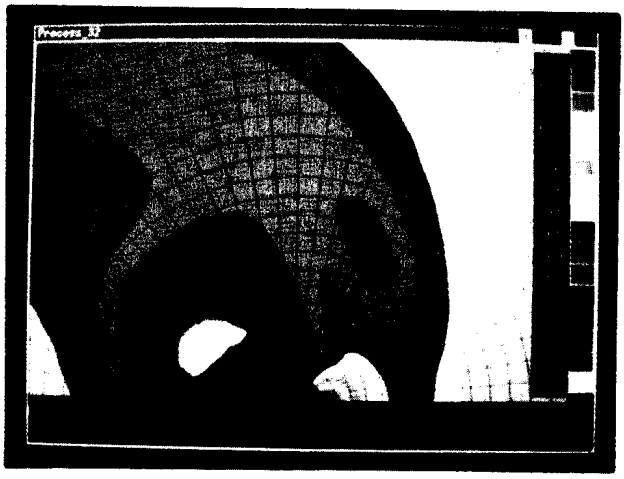

(b) Pressure distribution

Figure 24. Mach number and pressure distribution in the cross-flow plane for MISSILE(2) at M= 1.2, α= 22.5 deg. and zero roll. X/D = 14.06 (J= 27).

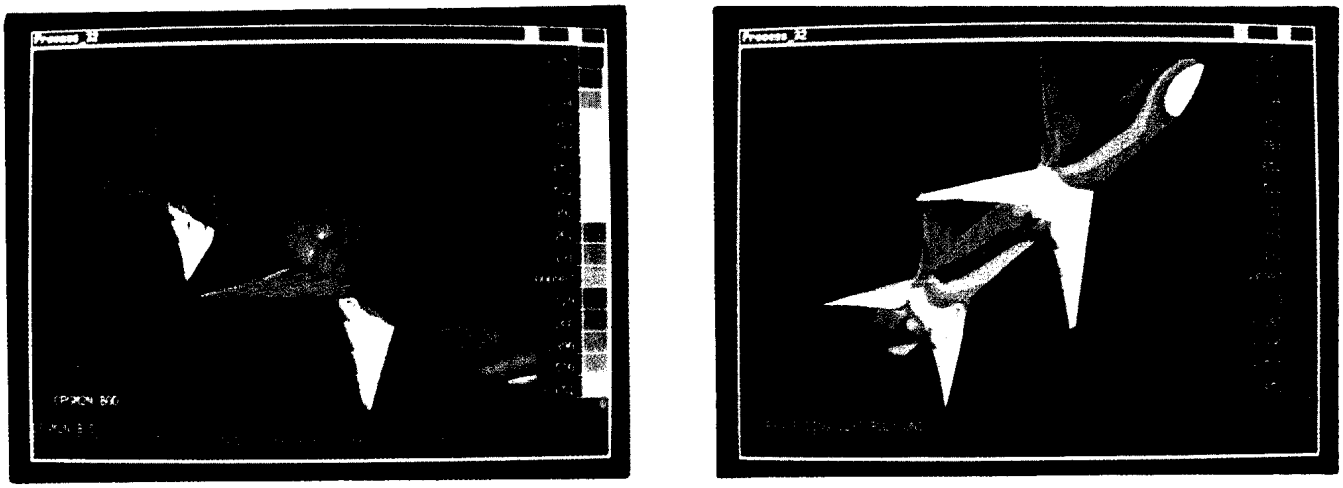

(a) Leeward side (b) Windward side

Figure 25. Distribution of surface pressure coefficients for MIS.SILE(2) at M= 1.2, α= 22.5 deg. and zero roll.

REFERENCES

1. M.R. Mendenhall and S.C. Perkins Jr.: Vortex cloud model for body vortex shedding and tracking, in "Tactical Missile Aerodynamics," ed. M.J. Hemsch and J.H. Nielsen, *AIAA Progress in Astronautics and Aeronautics*, Vol. 104, (1986).
2. G.H. Klopfer and J.H Nielsen : Euler solutions for wing and wing-body combination at supersonic speeds with leading-edge separation, *AIAA* paper 80-126.
3. A.B. Wardlaw Jr., F.J. Priolo and J.M Solomon: Multiple-Zone Strategy for Supersonic Missiles. *Journal of Spacecraft and Rockets*, Vol. 24, July-Aug. (1987).
4. F.J. Priolo and A.B. Wardlaw Jr.: Supersonic non-circular missile computations, *AIAA* paper 88-0278, Jan. (1988).
5. F.J. Priolo and A.B. Wardlaw Jr.: Induced roll computations for conventional missiles, *AIAA* paper 89-0331, January (1989).
6. F. Marconi. and G. Wilson: The computation of boundary region using the thin-layer navier-Stokes equations, *AIAA* paper 88-0231.
7. R.W. Newsome and M.S. Adams: Numerical simulation of vortical-flow over an elliptical-body missile at high angles of attack, *AIAA* paper 86-0559, Jan. (1986).
8. J. Deese, R. Agarwal and T. Gielda : Computation of supersonic viscous flow about missiles and bodies at high angles of attack using PNS and Navier-Stokes solvers, *AIAA* paper 89-0527, Jan, (1989).
9. T.H. Pulliam: Euler and thin-layer navier-stokes codes: ARC2D, ARC3D, notes for Computational Fluid Dynamics Users Workshop, The University of Tennessee Space Institute, Tullahoma, Tennessee, March 12-16, (1984).
10. R. Beam and R.F Warming: An implicit finite-difference algorithm for hyperbolic systems in Conservation-law-form, *Journal of Computational Physics*, Vol. 22, pp. 87-110, Sep. (1976).
11. T.H. Pulliam: Artificial dissipation models for the Euler equations, *AIAA* Vol. 24, No. 12, p. 1931, (1986).
12. J.L. Steger: Implicit finite difference simulation of flow about arbitrary geometries with application to airfoils, *AIAA* Vol. 16, p 679, July (1978).
13. J.F. Thompson: A composite grid generation code for general three-dimensional regions, AIAA 25th Aerospace Sciences Meeting. *AIAA* 87-0275.
14. J.J. Dongarra: Performance of various computers using standard linear equations software in a fortran environment, Argonne National Laboratory, TM No. 23 March (1988).
15. M. Lamb and C.D. Trescot: A study of panel loads and centers of pressure of three different cruciform aft-tail control surfaces of a wingless missile from Mach 1.60 to 3.70. *NASA*, TM 81787, (1980).
16. W.J. Monta: Supersonic aerodynamic characteristics of a sparrow III type missile model with wing controls and comparison with existing tail control results. *NASA*, TP-1078, (1977).